A 'best points' interpolation method for efficient approximation of parametrized functions

N. C. Nguyen*, †, A. T. Patera and J. Peraire

Massachusetts Institute of Technology, Cambridge, MA 20139, U.S.A.

SUMMARY

We present an interpolation method for efficient approximation of parametrized functions. The method recognizes and exploits the low-dimensional manifold structure of the parametrized functions to provide good approximation. Basic ingredients include a specific problem-dependent basis set defining a low-dimensional representation of the parametrized functions, and a set of 'best interpolation points' capturing the spatial-parameter variation of the parametrized functions. The best interpolation points are defined as solution of a least-squares minimization problem which can be solved efficiently using standard optimization algorithms. The approximation is then determined from the basis set and the best interpolation points through an inexpensive and stable interpolation procedure. In addition, an *a posteriori* error estimator is introduced to quantify the approximation error and requires little additional cost. Numerical results are presented to demonstrate the accuracy and efficiency of the method. Copyright © 2007 John Wiley & Sons, Ltd.

1. INTRODUCTION

Interpolation theory constitutes an active research area of mathematics and is relevant in various engineering and science applications such as numerical analysis and solution methods for partial differential equations (PDEs), computer graphics, medical imaging, signal processing, data mining, and artificial intelligence. The fundamental problem of interpolation theory is to approximate

*Correspondence to: N. C. Nguyen, Room 37-435, 77 Massachusetts Avenue, Cambridge, MA 02139, U.S.A.
†E-mail: cuongng@mit.edu

WILEY
InterScience®
DISCOVER SOMETHING GREAT

a given function by a simpler, easier-to-compute function residing in an approximation space spanned by a set of basis functions. An assumption often made is that the values of the function are known *a priori* at some points; the approximate function is then constructed from this information. Typically, classical interpolation methods (such as polynomial-based approaches) construct the approximate function by fitting the points to a linear combination of polynomials. Rather than the interpolation of general functions, we focus our investigation on the interpolation of parametrized functions, which is of considerable interest in many applications and merits a dedicated approach.

Specifically, in this paper, we are concerned with the interpolation of a parametrized function $u(x; \mu)$ defined on Ω for any given $\mu \in \mathscr{D}$. Here $\Omega \in \mathbb{R}^d$ is the physical domain with spatial coordinate x, and $\mathscr{D} \in \mathbb{R}^P$ is the parameter space in which our P-tuple parameter μ resides. Note that time-dependent functions can also be considered in this setting by including *time* in the parameter μ.

Our goal is the development of an interpolation method for efficient approximation of parametrized functions. The foundation of our method is built upon two important realizations. The first realization is that the manifold $\mathscr{M}^u \equiv \{u(x; \mu) \mid \mu \in \mathscr{D}\}$ is typically low dimensional and can thus be represented very well by a finite subset of basis functions. More precisely, rather than general basis sets such as polynomials, we construct a specific problem-dependent basis set with superior approximation properties. The second realization is that although $u(x; \mu)$ is defined on the entire physical domain Ω, its spatial-parameter variation may be captured by a limited number of 'selected' points in Ω. We exploit this observation to develop interpolation points that are best for the approximation of $u(x; \mu)$ for μ in $\mathscr{D}$. A function approximating $u(x; \mu)$ is then determined from the basis set and the interpolation points through an inexpensive and stable interpolation procedure. In addition, we provide an *a posteriori* error estimator to quantify the approximation error. Although our error estimator lacks theoretical rigor, it is quite sharp in practice and requires little additional cost.

As we emphasize on computational feasibility and effectiveness, we shall not pursue a comprehensive analysis in this paper. Nevertheless, we would like to point out the usefulness of our method in practical applications. The method may allow for an accurate and efficient reconstruction of a physical field such as displacement, temperature, or fluid velocity from experimental data collected at a few optimal sensor locations. In a numerical example presented in this paper, we shall describe in detail how the method applies to such problems. Another application is the construction of quadrature formulas for numerical integration of parametrized functions, which may be useful for the numerical solution of differential equations. Also, face recognition is a very important application in image analysis and computer vision, where the method may be gainfully employed [1]. In addition, the method can be effectively used to develop efficient reduced-basis approximation of nonaffine and non-linear parametrized PDEs [2].

In function interpolation by polynomials, aside from the smoothness of the functions to be interpolated, the interpolation points are critical to the convergence and accuracy of the approximation. A standard quality measure of an interpolation point set is the Lebesgue constant [3–5]. In one dimension, the Lebesgue-optimal point set and other optimal interpolation point sets in various measures have been developed [6–8], and their properties are well understood. In higher dimension, however, little is known concerning the Lebesgue-optimal interpolation point set. Therefore, many authors [6, 9–14] have investigated (near) optimal point sets defined by the solution of certain optimization problems. The interpolation point sets developed therein have been very useful to the construction of quadrature formulas and high-order shape functions in finite element analysis and

spectral methods. However, for the approximation of parametrized functions, these point sets are suboptimal, since they do not incorporate knowledge of the parametrized functions. Furthermore, their numerical computation is challenging especially when the size of the set is large. The main reason may be due to the fact that the associated optimization problems are generally difficult to solve.

Recently, Maday *et al.* [15–17] introduced the *empirical interpolation method* (EIM) that also deals with the interpolation of parametrized functions. The method has been incorporated into the reduced-basis techniques to provide efficient reduced-basis treatment of nonaffine and non-linear parametrized PDEs [15, 16, 18]. The main ingredients of the EIM are maximally independent basis functions and well-selected interpolation points (which we shall call the EIM points). A coefficient-function expansion approximating $u(x; \mu)$ is then obtained by an inexpensive and stable interpolation procedure. Although the EIM is very simple in implementation, it yields good performance in most cases.

In this paper, we shall compare our method with the EIM. The EIM is included in Appendix A.1 for reference. Our method differs from the EIM in the selection of the interpolation points. More specifically, while the EIM points are constructed by induction on the basis set, our interpolation points are determined from a least-squares minimization problem involving both the basis set and a family of known functions that characterizes the manifold $\mathcal{M}^u$. The EIM points are inexpensive and hierarchical, but they are not selected optimally.

The paper is organized as follows. In Section 2, we develop our best points interpolation method. In Section 3, we present *a priori* and *a posteriori* error analyses. In Section 4, we provide numerical examples to illustrate several features of the method, with special emphasis on application of the method to optimal sensor placement for reconstruction of a flow field. Finally, in Section 5, we close the paper with concluding remarks.

2. BEST POINTS INTERPOLATION METHOD

2.1. Interpolation problem

2.1.1. Problem description. We assume that we are given an approximation space consisting of N orthonormal basis functions, $\Phi_N = \text{span}\{\phi_1, \ldots, \phi_N\}$, with $(\phi_i, \phi_j) = \delta_{ij}$, $1 \leqslant i, j \leqslant N$; here δ is the Kronecker symbol and $(\cdot, \cdot)$ denotes an appropriate inner product with an induced norm $\| \cdot \| = \sqrt{(\cdot, \cdot)}$. Since we wish to approximate $u(\cdot; \mu)$ by a function $u_N(\cdot; \mu) \in \Phi_N$, it is crucial to equip the basis functions $\{\phi_n\}_{n=1}^N$ with good approximation properties.

The interpolation problem we aim to address is to find a set of N interpolation points, $Z_N = \{z_1 \in \Omega, \ldots, z_N \in \Omega\}$, that yields a *good* approximation[‡] $u_N(\cdot; \mu) \in \Phi_N$ to any $u(\cdot; \mu) \in \mathcal{M}^u$. Here, $u_N(x; \mu)$ is the 'coefficient-function' approximation determined by the following interpolation formula:

$$u_N(x; \mu) = \sum_{n=1}^N \beta_{Nn}(\mu) \phi_n(x) \tag{1}$$

[‡]By 'good approximation', we mean that our approximation $u_N(\cdot; \mu)$ is very close to the best approximation $u_N^*(\cdot; \mu) \in \Phi_N$ for all μ in $\mathcal{D}$. The best approximation $u_N^*(\cdot; \mu)$ is introduced below.

where the coefficients $\beta_{Nn}(\mu)$ are the solution of

$$\sum_{n=1}^{N} \phi_n(z_m)\beta_{Nn}(\mu) = u(z_m; \mu), \quad m = 1, \ldots, N \tag{2}$$

We define the associated error as

$$\varepsilon_N(\mu) \equiv \|u(\cdot; \mu) - u_N(\cdot; \mu)\| \tag{3}$$

We observe from (1)–(2) that $u_N(\cdot; \mu)$ and $u(\cdot; \mu)$ are equal at the interpolation points $\{z_n\}_{n=1}^{N}$.

2.1.2. Best approximation. We shall measure the quality of our coefficient-function approximation $u_N(\cdot; \mu)$ with respect to the best approximation $u_N^*(\cdot; \mu)$. The best approximation is defined as

$$u_N^*(\cdot; \mu) = \arg \min_{w_N \in \Phi_N} \|u(\cdot; \mu) - w_N\| \tag{4}$$

It is easily derived from the orthonormality of the ϕ_n that

$$u_N^*(x; \mu) = \sum_{n=1}^{N} \alpha_{Nn}(\mu)\phi_n(x) \tag{5}$$

where the coefficients are given by

$$\alpha_{Nn}(\mu) = (\phi_n, u(\cdot; \mu)), \quad n = 1, \ldots, N \tag{6}$$

The associated error is defined as

$$\varepsilon_N^*(\mu) \equiv \|u(\cdot; \mu) - u_N^*(\cdot; \mu)\| \tag{7}$$

We see that evaluation of the coefficients $\alpha_{Nn}(\mu)$, $1 \leqslant n \leqslant N$, requires the full knowledge of $u(x; \mu)$. Hence, approximating $u(x; \mu)$ by the best approximation $u_N^*(x; \mu)$ can be quite expensive and not a relevant approach in many practical contexts.

2.1.3. Remarks. In approximating the parametrized function $u(x; \mu)$, the critical observation is that the manifold $\mathcal{M}^u \equiv \{u(x; \mu) \mid \mu \in \mathscr{D}\}$ induced by the parametric dependence is typically low dimensional. We explicitly exploit dimension reduction afforded by the low-dimensional manifold to construct a specific problem-dependent basis set $\{\phi_n\}_{n=1}^{N}$ which is extremely effective for the approximation of functions in $\mathcal{M}^u$. More specifically, the set $\{\phi_n\}_{n=1}^{N}$ is constructed directly upon a family of (linearly independent) functions $\mathscr{U}_K = \{\zeta_k(x), 1 \leqslant k \leqslant K\}$, where $\zeta_k = u(x; \mu_k)$ for $\mu_k \in \mathscr{D}$. Typically, the sample set $S_K = \{\mu_1, \ldots, \mu_K\}$ is chosen such that any $u(\cdot; \mu) \in \mathcal{M}^u$ can be approximated very well by a linear combination of the ζ_k: for any $\mu \in \mathscr{D}$, there exist coefficients $c_k(\mu)$, $1 \leqslant k \leqslant K$, such that $\sum_{k=1}^{K} c_k(\mu)\zeta_k(x)$ is very close to $u(x; \mu)$.

We will describe here two different approaches for constructing $\{\phi_n\}_{n=1}^{N}$ from $\{\zeta_k\}_{k=1}^{K}$. One approach is to use the greedy selection process outlined in Appendix A.1 to generate maximally independent basis functions which are then orthonormalized by using the Gram–Schmidt orthonormalization. The other approach is to employ the Karhunen–Loève (KL) expansion [19] to generate an orthonormal basis set which is known to be optimal for representation of the family $\{\zeta_k\}_{k=1}^{K}$.

The details of the KL expansion are given in Appendix A.2 for reference. The two approaches result in two different basis sets. Due to its optimality property in the mean square error sense, the KL basis is superior to the greedy basis in the mean (norm). However, the KL basis can be more computationally expensive than the greedy basis because it necessitates $K(K+1)/2$ inner products and a singular value decomposition of a $K \times K$ *full* matrix.

Of course, the quality of our approximation depends critically not only on the basis functions but also on the interpolation points. At the very least, the interpolation points $\{z_n\}_{n=1}^N$ must be chosen such that the matrix $A^N \in \mathbb{R}^{N \times N}$ with $A_{mn}^N = \phi_n(z_m)$, $1 \leqslant m, n \leqslant N$, is invertible. In this case, the set of interpolation points $Z_N = \{z_1, \ldots, z_N\}$ is said to be *admissible*. The invertibility of A^N guarantees uniqueness of our coefficient-function approximation $u_N(x; \mu)$. The existence of admissible interpolation points follows directly from the linear independence of the basis set. However, for numerical stability, the interpolation points should be chosen such that A^N is well conditioned. At this point, one can think of finding a set of interpolation points that maximizes the determinant of A^N. The resulting interpolation points are the so-called Fekete points. However, the Fekete points do not necessarily give good approximation, since they do not exploit maximal information of the manifold $\mathcal{M}^u$.

2.2. Selection of interpolation points

In this section, we describe our approach for determining $\{z_n\}_{n=1}^N$ so as to provide a uniformly good approximation $u_N(\cdot; \mu)$ to $u(\cdot; \mu)$ for all $\mu \in \mathcal{D}$. Indeed, we shall propose not one but three different sets of interpolation points. The first set of points is optimal in the sense that it minimizes the sum of squared errors between the coefficient-function approximations and members of the family $\mathcal{U}_K$. The second set is also optimal in a slightly different sense. The third set of points is not optimal but hierarchical. The numerical difficulty in obtaining these sets of interpolation points is decreased in that order. Although we discuss the first set, we do not consider it in our numerical examples.

2.2.1. Optimal interpolation points.
We first introduce a concept of optimality for the interpolation points. The set of interpolation points is said to be *optimal* if it is the minimizer of the following minimization problem:

$$\min_{z_1 \in \Omega, \ldots, z_N \in \Omega} \int_{\mathcal{D}} \left\| u(\cdot; \mu) - \sum_{n=1}^N \beta_{Nn}(z_1, \ldots, z_N; \mu)\phi_n \right\|^2 d\mu$$

$$\sum_{n=1}^N \phi_n(z_m)\beta_{Nn} = u(z_m; \mu), \quad 1 \leqslant m \leqslant N, \quad \mu \in \mathcal{D} \tag{8}$$

$$\{z_m\}_{m=1}^N \text{ is admissible}$$

The above objective means minimizing the squared error averaged over the parameter space $\mathcal{D}$ and thus guarantees optimality in that sense. Unfortunately, solution of the above problem is not possible because the integral taken over the parameter space makes it impossible to evaluate the objective, let alone the computation of its gradients and Hessian. Rather than the integral, we may replace the objective in (8) with a 'min–max' objective $\min_{z_1 \in \Omega, \ldots, z_N \in \Omega} \max_{\mu \in \mathcal{D}} \| u(\cdot; \mu) - \sum_{n=1}^N \beta_{Nn}(z_1, \ldots, z_N; \mu)\phi_n \|$. Nevertheless, the resulting problem is still intractable for the same reason.

To obtain a tractable problem, we replace the integral with the sum of squared errors over the family $\mathcal{U}_K$ to arrive at

$$\min_{z_1 \in \Omega, \ldots, z_N \in \Omega} \sum_{k=1}^{K} \left\| \zeta_k - \sum_{n=1}^{N} \beta_{Nn}^k(z_1, \ldots, z_N)\phi_n \right\|^2$$

$$\sum_{n=1}^{N} \phi_n(z_m)\beta_{Nn}^k = \zeta_k(z_m), \quad 1 \leqslant m \leqslant N, \quad 1 \leqslant k \leqslant K \tag{9}$$

$$\{z_m\}_{m=1}^{N} \text{ is admissible}$$

Let us denote by $Z_N^{op} = \{z_1^{op}, \ldots, z_N^{op}\}$ the minimizer of problem (9). This set is optimal for the approximation of the family $\mathcal{U}_K$. Nevertheless, solution of the minimization problem (9) is difficult, because the problem is non-linear and nonconvex with (possibly) multiple local minima, and the Hessian is not easily computed. Below we introduce another set of points which can be computed more easily than the optimal interpolation points.

2.2.2. Best interpolation points. To begin, we introduce a family of functions $\mathcal{U}_K^* = \{\zeta_N^{*k}(x), 1 \leqslant k \leqslant K\}$, where ζ_N^{*k} is the best approximation to ζ_k. It thus follows that

$$\zeta_N^{*k}(x) = \sum_{n=1}^{N} \alpha_{Nn}^k \phi_n(x) \tag{10}$$

for $k = 1, \ldots, K$, where

$$\alpha_{Nn}^k = (\phi_n, \zeta_k), \quad 1 \leqslant n \leqslant N \tag{11}$$

We next replace ζ_k in the objective of problem (9) with ζ_N^{*k} to obtain

$$\min_{z_1 \in \Omega, \ldots, z_N \in \Omega} \sum_{k=1}^{K} \left\| \sum_{n=1}^{N} \alpha_{Nn}^k \phi_n - \sum_{n=1}^{N} \beta_{Nn}^k(z_1, \ldots, z_N)\phi_n \right\|^2$$

$$\sum_{n=1}^{N} \phi_n(z_m)\beta_{Nn}^k = \zeta_k(z_m), \quad 1 \leqslant m \leqslant N, \quad 1 \leqslant k \leqslant K \tag{12}$$

$$\{z_m\}_{m=1}^{N} \text{ is admissible}$$

By expanding the objective and invoking the orthonormality of $\{\phi_n\}_{n=1}^{N}$, we obtain

$$\min_{z_1 \in \Omega, \ldots, z_N \in \Omega} \sum_{k=1}^{K} \sum_{n=1}^{N} (\alpha_{Nn}^k - \beta_{Nn}^k(z_1, \ldots, z_N))^2$$

$$\sum_{n=1}^{N} \phi_n(z_m)\beta_{Nn}^k = \zeta_k(z_m), \quad 1 \leqslant m \leqslant N, \quad 1 \leqslant k \leqslant K \tag{13}$$

$$\{z_m\}_{m=1}^{N} \text{ is admissible}$$

Let us denote by $Z_N^{bp} = \{z_1^{bp}, \ldots, z_N^{bp}\}$ the minimizer of the above problem. We shall call these points as the best interpolation points or 'best points' for short.

Some remarks are useful. As regards the optimality property, problem (9) means minimizing the sum of squared errors between the coefficient-function approximations and members of family $\mathscr{U}_K$, whereas problem (13) means minimizing the sum of squared errors between the coefficient-function approximations and members of the family $\mathscr{U}_K^*$. In other words, while $\{z_n^{\mathrm{op}}\}_{n=1}^N$ is optimal for the approximation of the family $\mathscr{U}_K$, $\{z_n^{\mathrm{bp}}\}_{n=1}^N$ is optimal for the approximation of the family $\mathscr{U}_K^*$. As regards the existence and uniqueness of $\{z_n^{\mathrm{bp}}\}_{n=1}^N$, since the basis functions ϕ_n are linearly independent, there exists at least one admissible set of interpolation points. The existence of $\{z_n^{\mathrm{bp}}\}_{n=1}^N$ thus follows. However, uniqueness is not guaranteed. In general, there can be several sets of best points.

Most importantly, the non-linear least-squares minimization (13) is more efficient to solve than its counterpart (9) in the sense that the Hessian for (13) is much easier to compute than that for (9). As described in Section 2.3, the Levenberg–Marquardt (LM) algorithm is particularly well suited to solving (13).

2.2.3. Hierarchical interpolation points. In addition, we propose a set of hierarchical interpolation points ('hierarchical' points for short) $Z_N^{\mathrm{hp}} = \{z_1^{\mathrm{hp}}, \ldots, z_N^{\mathrm{hp}}\}$ which is less expensive to construct than Z_N^{bp}. Furthermore, a nice property of this set is that $Z_{N-1}^{\mathrm{hp}} \subset Z_N^{\mathrm{hp}}$. This hierarchical relation makes the set itself convenient in the *a posteriori* error estimation and in applications.

We construct Z_N^{hp} by solving a sequence of minimization problems. We first set $Z_1^{\mathrm{hp}} = \{z_1^{\mathrm{hp}}\}$, where z_1^{hp} is the minimizer of the following problem:

$$
\min_{z \in \Omega} \sum_{k=1}^K (\alpha_{N1}^k - \beta_{11}^k(z))^2
$$

$$
\phi_1(z)\beta_{11}^k = \zeta_k(z), \quad 1 \leqslant k \leqslant K \tag{14}
$$

$$
\{z\} \text{ is admissible}
$$

Then, for $L = 2, \ldots, N$, we find and append z_L^{hp} to Z_{L-1}^{hp} to form Z_L^{hp}, where z_L^{hp} is the minimizer of

$$
\min_{z \in \Omega} \sum_{k=1}^K \sum_{\ell=1}^L (\alpha_{N\ell}^k - \beta_{L\,\ell}^k(z))^2
$$

$$
\sum_{l=1}^L \phi_l(z_m^{\mathrm{hp}})\beta_{Ll}^k = \zeta_k(z_m^{\mathrm{hp}}), \quad 1 \leqslant m \leqslant L-1, \quad 1 \leqslant k \leqslant K
$$

$$
\sum_{l=1}^L \phi_l(z)\beta_{Ll}^k = \zeta_k(z), \quad 1 \leqslant k \leqslant K \tag{15}
$$

$$
z \text{ such that } \{z_1^{\mathrm{hp}}, \ldots, z_{L-1}^{\mathrm{hp}}, z\} \text{ is admissible}
$$

In this way, each of the problems has only one variable z and can thus be easily solved for a global solution.

2.3. Solution procedure

We now find a solution of the least-squares minimization problem (13) using the LM algorithm. For simplicity of exposition, we consider $\Omega \subset \mathbb{R}^1$. Higher-dimensional cases can be treated in a similar manner.

We first write problem (13) in the form

$$\min F(s) = \frac{1}{2} \sum_{q=1}^{Q} f_q^2(s)$$

$$s = (z_1 \in \Omega, \ldots, z_N \in \Omega)^{\mathrm{T}} \subset \mathbb{R}^N \tag{16}$$

where $f_q(s)$, $1 \leqslant q \leqslant Q = KN$, are given by

$$f_q(s) = \alpha_{Nn}^k - \beta_{Nn}^k(s), \quad 1 \leqslant k \leqslant K, \quad 1 \leqslant n \leqslant N \tag{17}$$

The gradient and Hessian of the objective function $F(s)$ can thus be computed as

$$\nabla F(s) = \sum_{q=1}^{Q} f_q(s) \nabla f_q(s) = J(s)^{\mathrm{T}} f(s) \tag{18}$$

$$\nabla^2 F(s) = J(s)^{\mathrm{T}} J(s) + \sum_{q=1}^{Q} f_q(s) \nabla^2 f_q(s) \tag{19}$$

where for $1 \leqslant q \leqslant Q$, $1 \leqslant n \leqslant N$,

$$J_{qn}(s) = \frac{\partial f_q(s)}{\partial z_n} = \frac{\partial \beta_{Nn}^k(s)}{\partial z_n} \tag{20}$$

Hence, when the residuals $f_q(s)$ are small, we may approximately compute the Hessian in terms of only the Jacobian matrix $J(s)$ as

$$\nabla^2 F(s) = J(s)^{\mathrm{T}} J(s) \tag{21}$$

In practice, the Hessian is often computed using this approximation to reduce the computational cost. (Throughout the paper, we shall use (21) to obtain the Hessian.) However, whenever the second partial derivatives $\nabla^2 f_q(s)$ are available with reasonable cost, the whole formula (19) should be used to render more rapid convergence to a global solution, especially for large residual problems.

To compute the Jacobian matrix $J(s)$, we note from (2) that

$$\frac{\partial \beta_N^k}{\partial z_n} = (A^N)^{-1} \left(\frac{\partial b_N^k}{\partial z_n} - \frac{\partial A^N}{\partial z_n} \beta_N^k \right) \tag{22}$$

where for $k = 1, \ldots, K$, $\beta_N^k = (\beta_{N1}^k, \ldots, \beta_{NN}^k)^{\mathrm{T}} \in \mathbb{R}^N$, $b_N^k = (u_k(z_1), \ldots, u_k(z_N))^{\mathrm{T}} \in \mathbb{R}^N$, $\partial b_N^k / \partial z_n \in \mathbb{R}^N$ has only one nonzero element equal to $\partial u_k(z_n)/\partial x$ at the index n, and $\partial A^N / \partial z_n \in \mathbb{R}^{N \times N}$ has only one nonzero row equal to $(\partial \phi_1(z_n)/\partial x, \ldots, \partial \phi_N(z_n)/\partial x)$ at the nth row. Note further that $\{\partial \phi_n/\partial x\}_{n=1}^N$ can be calculated from $\{\partial \zeta_k/\partial x\}_{k=1}^K$ *via* relationship (A6).

Having determined the gradient and the Hessian, the LM algorithm [20] can now be applied to solve (13) for the best points. The LM algorithm is very efficient, but quite sensitive to the initial guess. Multi-start strategies can thus be effectively used to achieve a global minimizer. In our actual implementation, we start the algorithm with two different initial solutions. The first initial solution is the set of hierarchical points $\{z_n^{\mathrm{hp}}\}_{n=1}^N$. The second initial solution is the set $Z_N^{\mathrm{ip}} = \{z_1^{\mathrm{ip}}, \ldots, z_N^{\mathrm{ip}}\}$ calculated as follows: we set $z_1^{\mathrm{ip}} = \arg \operatorname{ess\,sup}_{x \in \Omega} |\phi_1(x)|$; then for $L = 2, \ldots, N$, we solve the linear system $\sum_{j=1}^{L-1} \phi_j(z_i^{\mathrm{ip}}) \sigma_j^{L-1} = \phi_L(z_i^{\mathrm{ip}})$, $1 \leqslant i \leqslant L-1$, and set $r_L(x) = \phi_L(x) - \sum_{j=1}^{L-1} \sigma_j^{L-1} \phi_j(x)$, $z_L^{\mathrm{ip}} = \arg \operatorname{ess\,sup}_{x \in \Omega} |r_L(x)|$. These are essentially the EIM points associated with the basis set $\{\phi_n\}_{n=1}^N$.

In summary, the best points $\{z_n^{\mathrm{bp}}\}_{n=1}^N$ and the hierarchical points $\{z_n^{\mathrm{hp}}\}_{n=1}^N$ are constructed by solving the associated error minimization problems. They enjoy optimality in various senses. Our interpolation formula (1)–(2) can now be carried out with the set of interpolation points $\{z_n\}_{n=1}^N$ being one of the two sets. This essentially produces an approximation $u_N(x; \mu)$ to $u(x; \mu)$ for any given $\mu \in \mathscr{D}$. It remains, however, to understand how well $u_N(x; \mu)$ approximates $u(x; \mu)$.

3. ERROR ANALYSIS

3.1. A priori framework

In interpolation theory, the Lebesgue constants [3–5] measure how good the approximation of a function is in comparison with the best approximation. We might follow [15, 16] to define a Lebesgue constant as

$$\Lambda_N = \sup_{x \in \Omega} \sum_{n=1}^N |\psi_n(x)| \tag{23}$$

Here, the $\psi_n \in \Phi_N$ are cardinal functions satisfying $\psi_m(z_n) = \delta_{mn}$, $1 \leqslant m, n \leqslant N$. It can then be shown in [15, 16] that

$$\|u(\cdot; \mu) - u_N(\cdot; \mu)\|_{L^\infty(\Omega)} \leqslant (1 + \Lambda_N) \|u(\cdot; \mu) - u_N^*(\cdot; \mu)\|_{L^\infty(\Omega)} \quad \forall \mu \in \mathscr{D}$$

However, Λ_N is too conservative as a quality measure for the approximation $u_N(x; \mu)$ of $u(x; \mu)$, since in fact $\|v - v_N\|_{L^\infty(\Omega)} \leqslant \|v - v_N^*\|_{L^\infty(\Omega)} (1 + \Lambda_N)$ is also true for any function $v \in L^\infty(\Omega)$. As a result, the Lebesgue constant Λ_N as defined above is quite large; furthermore, it is only applicable to the $L^\infty(\Omega)$ norm.

Hence, we introduce a different quality measure of the approximation $u_N(x; \mu)$ with respect to the best approximation $u_N^*(x; \mu)$ as

$$\Gamma_N = \max_{\mu \in \mathscr{D}} \frac{\varepsilon_N(\mu)}{\varepsilon_N^*(\mu)} \tag{24}$$

This implies

$$\varepsilon_N(\mu) \leqslant \Gamma_N \varepsilon_N^*(\mu) \quad \forall \mu \in \mathscr{D}$$

Typically, Γ_N is obtained by solving the maximization problem (24). We observe that Γ_N depends on Φ_N and Z_N, but not on μ. Note further that $\Gamma_N \geqslant 1$ and that a value of Γ_N close to unity indicates a very good approximation.

An estimate for the behavior of Γ_N as a function of N is of course fundamental for the study of the convergence properties of our method. This suggests an interesting theoretical investigation for future work.

3.2. A posteriori estimators

In order to be certain that our approximation satisfies the accuracy level of interest, we must have *a posteriori* error estimators. Indeed, the reliability of our approximation rests crucially on the *a posteriori* error estimators, without which the unquantified uncertainty may lead to erroneous predictions.

We first recall the following result from [16, Lemma 2.4].

Lemma 3.1
The set of all cardinal functions $\{\psi_n\}_{n=1}^N$ is a basis for Φ_N. Furthermore, the two bases ϕ_n, $1 \leqslant n \leqslant N$, and ψ_n, $1 \leqslant n \leqslant N$, are related by

$$\phi_i(x) = \sum_{j=1}^N A_{ji}^N \psi_j(x), \quad 1 \leqslant i \leqslant N \tag{25}$$

which immediately implies that $u_N(x; \mu)$ as defined by (1)–(2) satisfies

$$u_N(x; \mu) = \sum_{j=1}^N u(z_j; \mu) \psi_j(x) \tag{26}$$

Expression (26) clearly shows that when expressing $u_N(x; \mu)$ in terms of the cardinal basis set $\{\psi_n\}_{n=1}^N$, we do not need to solve a linear system for the coefficients as it is required for the case of using the basis set $\{\phi_n\}_{n=1}^N$. We thus suggest using the interpolation formula (26) rather than (1)–(2) for the coefficient-function approximation $u_N(x; \mu)$. Note, however, that the cardinal set $\{\psi_n\}_{n=1}^N$ depends on both $\{z_n\}_{n=1}^N$ and $\{\phi_n\}_{n=1}^N$ and is thus not a hierarchical basis. Furthermore, since $\{\psi_n\}_{n=1}^N$ is obtained by inverting A^N, it is important that the matrix A^N is well conditioned.

We now augment our current basis set $\{\phi_n\}_{n=1}^N$ with I basis functions $\{\phi_{N+1}, \ldots, \phi_{N+I}\}$ to form an approximation space Φ_{N+I} spanned by the extended basis set $\{\phi_n\}_{n=1}^{N+I}$. Associated with this extended basis set are the extended set of interpolation points $Z_{N,I} = \{\{z_n\}_{n=1}^N \cup \{z_{N,i}\}_{i=1}^I\}$ such that $Z_N \subset Z_{N,I}$ and set of cardinal basis functions $\{\psi_n\}_{n=1}^{N+I}$. We define an estimate for our approximation error $\varepsilon_N(\mu)$ as

$$\hat{\varepsilon}_{N,I}(\mu) = \sqrt{\sum_{i=1}^I \sum_{i'=1}^I e_i^u(\mu) e_{i'}^u(\mu) \sigma_{ii'}} \tag{27}$$

where

$$e_i^u(\mu) = u(z_{N,i}; \mu) - u_N(z_{N,i}; \mu), \quad \sigma_{ii'} = (\psi_{N+i}, \psi_{N+i'}), \quad 1 \leqslant i, i' \leqslant I \tag{28}$$

We can then prove the following proposition.

Proposition 1
If $u(\cdot; \mu) \in \Phi_{N+I}$ and $Z_N \subset Z_{N,I}$, then $\|u(\cdot; \mu) - u_N(\cdot; \mu)\| = \hat{\varepsilon}_{N,I}(\mu)$.

Proof
By our first assumption $u(\cdot; \mu) \in \Phi_{N+I}$, there exists $\kappa(\mu) \in \mathbb{R}^{N+I}$ such that $u(x; \mu) - u_N(x; \mu)$
$= \sum_{m=1}^{N+I} \kappa_m(\mu)\psi_m(x)$. We now consider $x = z_n$, $1 \leqslant n \leqslant N$, and $x = z_{N,i}$, $1 \leqslant i \leqslant I$, to obtain

$$\sum_{m=1}^{N+I} \kappa_m(\mu)\psi_m(z_n) = u(z_n; \mu) - u_N(z_n; \mu), \quad 1 \leqslant n \leqslant N$$

$$\sum_{m=1}^{N+I} \kappa_m(\mu)\psi_m(z_{N,i}) = u(z_{N,i}; \mu) - u_N(z_{N,i}; \mu), \quad 1 \leqslant i \leqslant I$$

It thus follows from our second assumption $Z_N \subset Z_{N,I}$ that $\kappa_n(\mu) = 0$, $1 \leqslant n \leqslant N$, and $\kappa_{N+i}(\mu) = u(z_{N,i}; \mu) - u_N(z_{N,i}; \mu)$, $1 \leqslant i \leqslant I$, since $u(z_n; \mu) - u_N(z_n; \mu) = 0$, $1 \leqslant n \leqslant N$, and $\psi_m(x_{m'}) = \delta_{mm'}$, $1 \leqslant m, m' \leqslant N + I$, for $x_n = z_n$, $1 \leqslant n \leqslant N$, and $x_{N+i} = z_{N,i}$, $1 \leqslant i \leqslant I$. Hence, we obtain $u(x; \mu) - u_N(x; \mu) = \sum_{i=1}^{I} (u(z_{N,i}; \mu) - u_N(z_{N,i}; \mu))\psi_{N+i}(x)$. The desired result immediately follows from definition of $\hat{\varepsilon}_{N,I}(\mu)$. $\qquad \square$

Of course, in general $u(\cdot; \mu) \notin \Phi_{N+I}$, and hence our error estimator $\hat{\varepsilon}_{N,I}(\mu)$ is unfortunately not a rigorous upper bound. However, if $\varepsilon_N(\mu) \to 0$ very fast, we expect that the effectivity

$$\eta_{N,I}(\mu) = \frac{\hat{\varepsilon}_{N,I}(\mu)}{\varepsilon_N(\mu)} \tag{29}$$

will be close to unity; furthermore, the estimator is very inexpensive with a computational cost of only $\mathcal{O}(I^2)$ when the quantities $\sigma_{ii'}$ are precomputed and stored.

Finally, we note that the hierarchical relation $Z_N \subset Z_{N+I}$ does hold for Z_N^{hp}, but not for Z_N^{bp}. Hence, we can set $Z_{N,I}^{\mathrm{hp}} = Z_{N+I}^{\mathrm{hp}}$. However, to form $Z_{N,I}^{\mathrm{bp}}$, we subsequently set $Z_{N,i}^{\mathrm{bp}} = Z_{N,i-1}^{\mathrm{bp}} \cup z_{N,i}^{\mathrm{bp}}$ (with $Z_{N,0}^{\mathrm{bp}} = Z_N^{\mathrm{bp}}$) for $i = 1, \ldots, I$, where $z_{N,i}^{\mathrm{bp}}$ is the solution of

$$\min_{z \in \Omega} \sum_{k=1}^{K} \sum_{n=1}^{N+i} (\alpha_{Nn}^k - \beta_{Nn}^k(z))^2$$

$$\sum_{n=1}^{N+i} \phi_n(z_j^{\mathrm{bp}})\beta_{Nn}^k = u_k(z_j^{\mathrm{bp}}), \quad 1 \leqslant j \leqslant N, \;\; 1 \leqslant k \leqslant K$$

$$\sum_{n=1}^{N+i} \phi_n(z_{N,j}^{\mathrm{bp}})\beta_{Nn}^k = u_k(z_{N,j}^{\mathrm{bp}}), \quad 1 \leqslant j \leqslant i - 1, \;\; 1 \leqslant k \leqslant K \tag{30}$$

$$\sum_{n=1}^{N+i} \phi_n(z)\beta_{Nn}^k = u_k(z), \quad 1 \leqslant k \leqslant K$$

z such that $\{z_1^{\mathrm{bp}}, \ldots, z_N^{\mathrm{bp}}, z_{N,1}^{\mathrm{bp}}, \ldots, z_{N,i-1}^{\mathrm{bp}}, z\}$ is admissible

Note that the above problem has only one variable z.

4. NUMERICAL EXAMPLES

In this section we apply our method to three numerical examples. The examples serve to illustrate several features of the method. In the first two examples, we present the results obtained with the best points and with the hierarchical points, compare the coefficient-function approximation with the best approximation and with that provided by the EIM, and show the convergence rate of the approximation error and the sharpness of the error estimator. In the last example, we demonstrate the application of our method to optimal sensor placement for reconstruction of a flow field. In all examples, we shall consider a very fine discretization of the spatial domain Ω and the usual Euclidean inner product for simplicity. Furthermore, the KL procedure is employed to construct the basis set $\{\phi_n\}_{n=1}^{N}$.

4.1. Example 1

Our first example is the exponentially decaying sinusoidal function of the form

$$G(x; \mu) = (1 - x) \cos(3\pi\mu(x + 1))e^{-(1+x)\mu} \tag{31}$$

defined on the interval $\Omega = [-1, 1]$. Here μ varies in the parameter domain $\mathscr{D} \equiv [1, \pi]$. As μ increases, we observe oscillation with higher frequency at a faster decaying rate as shown in Figure 1. Below we present numerical results for this example.

We first introduce a regular grid S_K of size $K = 51$ on the parameter space and the associated family $\mathscr{U}_K = \{\zeta_k(x) \equiv G(x; \mu_k) \mid \mu_k \in S_K, 1 \leqslant k \leqslant K\}$. Upon the family $\mathscr{U}_K$, we construct the approximation space $\Phi_N = \mathrm{span}\{\phi_1, \ldots, \phi_N\}$ following the KL procedure outlined in Appendix A.2. We present in Table I the coordinate values of the best points Z_N^{bp}, the hierarchical points Z_N^{hp}, and the EIM points Z_N^{mp} obtained using the EIM described in Appendix A.1. We observe that the interpolation points are mainly distributed on the left of the physical domain.
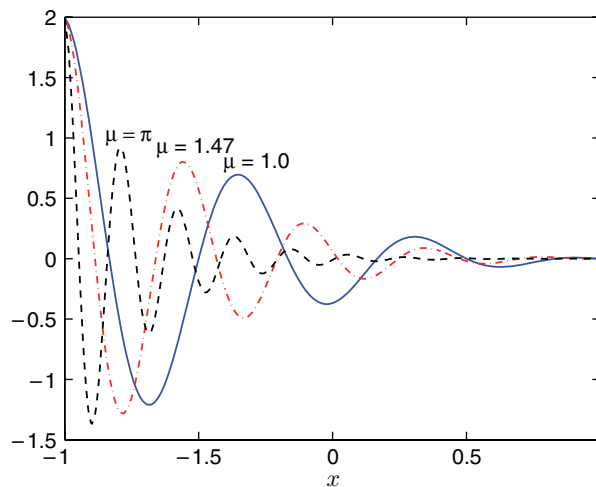

Figure 1. Behavior of $G(x; \mu)$ for different parameter values.

Table I. Coordinate values of the best points, hierarchical
points, and EIM points for $N = 12$.

n	Z_N^{bp}	Z_N^{hp}	Z_N^{mp}
1	-0.9562	-0.9659	-1.0000
2	-0.8862	-0.8832	-0.9098
3	-0.7080	-0.6527	-0.6680
4	-0.6140	-0.5665	-0.5462
5	-0.5036	-0.4776	-0.4776
6	-0.4242	-0.3839	-0.1679
7	-0.3139	-0.2917	-0.2555
8	-0.1127	-0.0511	$+0.1679$
9	$+0.0073$	$+0.0365$	-0.7321
10	$+0.0985$	$+0.0985$	$+0.2993$
11	$+0.3473$	$+0.3473$	$+0.0875$
12	$+0.4450$	$+0.3860$	$+0.5912$

Table II. Comparison of the BPIM, HPIM, and EIM: $\varepsilon_{N,\max,\text{rel}}$ and $\overline{\Upsilon}_N$ as a function of N.

N	BPIM		HPIM		EIM	
	$\varepsilon_{N,\max,\text{rel}}$	$\overline{\Upsilon}_N$	$\varepsilon_{N,\max,\text{rel}}$	$\overline{\Upsilon}_N$	$\varepsilon_{N,\max,\text{rel}}$	$\overline{\Upsilon}_N$
3	5.87E$-$01	1.01	6.02E$-$01	1.04	7.17E$-$01	1.63
6	2.07E$-$01	1.05	2.32E$-$01	1.19	4.95E$-$01	2.51
9	7.02E$-$02	1.11	9.10E$-$02	1.21	1.02E$-$01	1.72
12	1.39E$-$02	1.16	2.75E$-$02	1.50	4.32E$-$02	1.99
15	1.46E$-$03	1.20	3.65E$-$03	1.99	2.73E$-$03	1.64
18	7.46E$-$05	1.15	2.89E$-$04	2.84	2.13E$-$04	3.76

We now define $\varepsilon_{N,\max,\text{rel}} = \max_{\mu \in \Xi_{\text{Test}}} \varepsilon_N(\mu)/\|G(\cdot\,;\mu)\|$ and $\overline{\Upsilon}_N = Q_{\text{Test}}^{-1} \sum_{\mu \in \Xi_{\text{Test}}} \varepsilon_N(\mu)/$ $\varepsilon_N^*(\mu)$; here Ξ_{Test} is a parameter test sample of size $Q_{\text{Test}} = 101$. The maximum relative error $\varepsilon_{N,\max,\text{rel}}$ will show the convergence rate of the coefficient-function approximation. The average error ratio $\overline{\Upsilon}_N$ will measure the approximation quality relative to the best approximation—a value close to unity indicates a very good approximation. In Table II, we tabulate $\varepsilon_{N,\max,\text{rel}}$ and $\overline{\Upsilon}_N$ as a function of N using the best points (BPIM) and the hierarchical points (HPIM), and the EIM. As expected, the BPIM yields the best performance as it gives smallest values of $\varepsilon_{N,\max,\text{rel}}$ and $\overline{\Upsilon}_N$. Furthermore, while $\overline{\Upsilon}_N$ for the HPIM and EIM tends to grow with N, $\overline{\Upsilon}_N$ for the BPIM is very close to unity for all N. We also observe that $\overline{\Upsilon}_N$ for the HPIM grows at a faster rate for large N. This may be attributed to the fact that the set of hierarchical points is suboptimal and loses its optimality as N increases.

In addition, we tabulate in Table III $\varepsilon_{N,\max,\text{rel}}$, Γ_N, $\varkappa_N$, and $\overline{\eta}_{N,I}$, $1 \leqslant I \leqslant 3$, as a function of N for the best points; here $\overline{\eta}_{N,I} = Q_{\text{Test}}^{-1} \sum_{\mu \in \Xi_{\text{Test}}} \eta_{N,I}(\mu)$ and $\varkappa_N$ is the condition number of A^N. We observe from these results that the maximum relative error decreases very rapidly with N; that the constant Γ_N is less than two and grows very slowly—and hence $\varepsilon_N(\mu)$ will be *only slightly*

Table III. Numerical results for the approximation of $G(x; \mu)$ using the BPIM: $\varepsilon_{N,\max,\mathrm{rel}}$, Γ_N, $\varkappa_N$, and $\overline{\eta}_{N,I}$, $1 \leqslant I \leqslant 3$ as a function of N.

N	$\varepsilon_{N,\max,\mathrm{rel}}$	Γ_N	$\varkappa_N$	$\overline{\eta}_{N,1}$	$\overline{\eta}_{N,2}$	$\overline{\eta}_{N,3}$
3	5.87E−01	1.06	1.70	0.65	0.86	0.95
6	2.07E−01	1.30	2.59	0.68	0.92	0.98
9	7.02E−02	1.38	2.25	0.70	0.94	0.99
12	1.39E−02	1.63	3.36	0.70	0.95	0.99
15	1.46E−03	1.75	4.93	0.73	0.97	1.00
18	7.46E−05	1.72	4.29	0.81	0.98	1.00

Table IV. Numerical results for the approximation of $G(x; \mu)$ using the Legendre polynomials and the extended Chebyshev points: $\varepsilon_{N,\max,\mathrm{rel}}$ and $\overline{\Upsilon}_N$ as a function of N.

N	$\varepsilon_{N,\max,\mathrm{rel}}$	$\overline{\Upsilon}_N$
5	1.44E−00	1.37
10	9.59E−01	1.44
15	6.70E−01	1.35
20	4.11E−01	1.30
25	1.63E−01	1.25
30	3.72E−02	1.19
35	2.37E−03	1.13
40	4.06E−05	1.09

larger than the best approximation error $\varepsilon_N^*(\mu)$; that A^N is very well conditioned; and that the error estimator effectivity is quite close to unity and sharper as I increases.

Finally, we consider the interpolation of $G(x; \mu)$ using the Legendre polynomials and the extended Chebyshev points

$$z_n^{\mathrm{cp}} = \frac{\cos((2n-1)\pi/(2N))}{\cos(\pi/(2N))}, \quad n = 1, \ldots, N$$

We present in Table IV $\varepsilon_{N,\max,\mathrm{rel}}$ and $\overline{\Upsilon}_N$ as a function of N. We see that although the approximation is very close to the best approximation, the error converges much slower than those obtained with the BPIM, HPIM, and EIM. Hence, at least in this particular example, polynomial interpolation is not an effective approach.

4.2. Example 2

We consider a sinusoidal μ-dependent function $H(x; \mu) = \sin(\mu^1 x^1)\cos(\mu^2 x^2)$ defined on the physical domain $\Omega = [0,1] \times [0,1]$. Here, the parameter $\mu = (\mu^1, \mu^2)$ varies in $\mathcal{D} = [\pi/3, 2\pi] \times [\pi/3, 2\pi]$. The KL basis set $\{\phi_n\}_{n=1}^N$ is then constructed from the family $\mathcal{U}_K = \{\zeta_k(x) \equiv H(x; \mu_k) \mid \mu_k \in S_K, 1 \leqslant k \leqslant K\}$, where S_K is a regular grid of size $K = 441$ on the parameter space $\mathcal{D}$. Below we present numerical results obtained for this example.

Table V. Comparison of BP I, BP II, and BP III: $\varepsilon_{N,\max,\mathrm{rel}}$ and $\overline{\Upsilon}_N$ as a function of N.

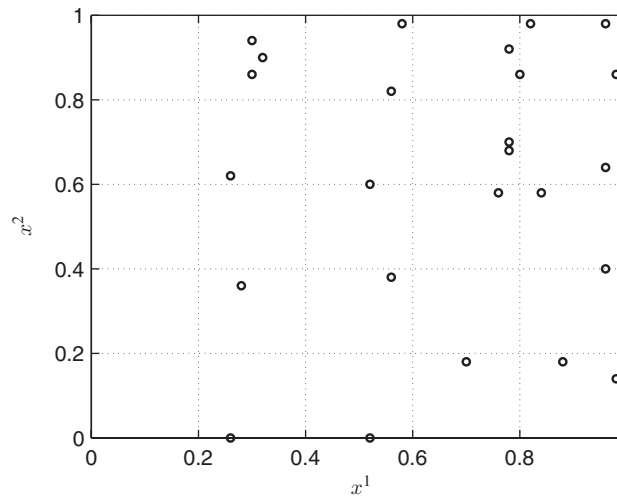|	BP I		BP II		BP III	
N	$\varepsilon_{N,\max,\mathrm{rel}}$	$\overline{\Upsilon}_N$	$\varepsilon_{N,\max,\mathrm{rel}}$	$\overline{\Upsilon}_N$	$\varepsilon_{N,\max,\mathrm{rel}}$	$\overline{\Upsilon}_N$
5	8.92E−01	1.10	8.92E−01	1.10	7.81E−01	1.02
10	1.30E−01	1.10	1.32E−01	1.10	1.20E−01	1.04
15	7.45E−03	1.16	6.66E−03	1.20	7.38E−03	1.09
20	9.81E−04	1.15	9.77E−04	1.15	9.34E−04	1.21
25	1.31E−04	1.19	1.34E−04	1.26	1.21E−04	1.16

Figure 2. Distribution of the best points on the physical domain for $N = 25$.

We first investigate the sensitivity of the solutions of (13) with respect to initial guesses. Here, we consider three different initial guesses: Z_N^{ip}, Z_N^{hp}, and a random set of points. For numerical stability, the random set is chosen so as to make A^N quite well conditioned. We denote by BP I, BP II, and BP III the three solutions corresponding to the three initial guesses. For this purpose, we introduce a parameter test sample Ξ_{Test} of size $Q_{\mathrm{Test}} = 961$. We present in Table V $\varepsilon_{N,\max,\mathrm{rel}}$ and $\overline{\Upsilon}_N$ as a function of N for BP I, BP II, and BP III; here $\varepsilon_{N,\max,\mathrm{rel}} = \max_{\mu \in \Xi_{\mathrm{Test}}} \varepsilon_N(\mu) / \|H(\cdot; \mu)\|$, $\Upsilon_N(\mu) = \varepsilon_N(\mu) / \varepsilon_N^*(\mu)$, and $\overline{\Upsilon}_N = Q_{\mathrm{Test}}^{-1} \sum_{\mu \in \Xi_{\mathrm{Test}}} \Upsilon_N(\mu)$. We observe that BP I, BP II, and BP III perform almost equally well since they yield similar convergence rates and average error ratios. We may thus conclude that in the particular example the results are not much affected by the choice of initial guesses.

We now let the set of best points be the set among BP I, BP II, and BP III that gives the smallest objective value. Figure 2 shows distribution of the best points for 25 basis functions. We see that the best points are largely located around the upper right region of the physical domain. We further tabulate in Table VI $\varepsilon_{N,\max,\mathrm{rel}}$ and $\overline{\Upsilon}_N$ as a function of N for the BPIM, HPIM, and EIM. We see

Table VI. Comparison of the BPIM, HPIM, and EIM: $\varepsilon_{N,\max,\mathrm{rel}}$ and $\overline{\Upsilon}_N$ as a function of N.

	BPIM		HPIM		EIM	
N	$\varepsilon_{N,\max,\mathrm{rel}}$	$\overline{\Upsilon}_N$	$\varepsilon_{N,\max,\mathrm{rel}}$	$\overline{\Upsilon}_N$	$\varepsilon_{N,\max,\mathrm{rel}}$	$\overline{\Upsilon}_N$
5	7.81E−01	1.02	8.86E−01	1.11	2.21E−00	4.70
10	1.20E−01	1.04	1.29E−01	1.27	5.01E−01	7.42
15	7.38E−03	1.09	9.81E−03	1.77	2.97E−02	5.24
20	9.81E−04	1.15	2.90E−03	3.23	3.30E−03	7.40
25	1.21E−04	1.16	5.20E−04	4.63	4.38E−04	8.51

Table VII. Numerical results for the approximation of $H(x;\mu)$ using the BPIM: $\varepsilon^{*}_{N,\max,\mathrm{rel}}$, $\varepsilon_{N,\max,\mathrm{rel}}$, Γ_N, $\varkappa_N$, and $\overline{\eta}_{N,I}$, $1\leqslant I\leqslant 3$, as a function of N.

N	$\varepsilon^{*}_{N,\max,\mathrm{rel}}$	$\varepsilon_{N,\max,\mathrm{rel}}$	Γ_N	$\varkappa_N$	$\overline{\eta}_{N,1}$	$\overline{\eta}_{N,2}$	$\overline{\eta}_{N,3}$
5	7.76E−01	7.81E−01	1.33	1.67	0.63	0.90	0.97
10	1.19E−01	1.20E−01	1.77	2.28	0.76	0.91	0.95
15	5.95E−03	7.38E−03	1.63	2.69	0.58	0.82	0.94
20	8.46E−04	9.81E−04	1.83	3.90	0.63	0.87	0.94
25	1.11E−04	1.21E−04	1.56	120	0.59	0.79	0.93

again that the BPIM yields the best performance and that while $\overline{\Upsilon}_N$ for the HPIM and EIM tends to grow with N, $\overline{\Upsilon}_N$ for the BPIM is very close to unity for all N.

Finally, we present in Table VII $\varepsilon^{*}_{N,\max,\mathrm{rel}}$, $\varepsilon_{N,\max,\mathrm{rel}}$, Γ_N, $\varkappa_N$, and $\overline{\eta}_{N,I}$, $1\leqslant I\leqslant 3$, as a function of N for the BPIM; here $\varepsilon^{*}_{N,\max,\mathrm{rel}} = \max_{\mu\in\Xi_{\mathrm{Test}}}\varepsilon^{*}_N(\mu)/\|H(\cdot;\mu)\|$, $\overline{\eta}_{N,I} = Q^{-1}_{\mathrm{Test}}\sum_{\mu\in\Xi_{\mathrm{Test}}}\eta_{N,I}(\mu)$, and $\varkappa_N$ is the condition number of A^N. We see that $\varepsilon_{N,\max,\mathrm{rel}}$ converges very rapidly with N; that the constant Γ_N provides a sharp measure of the interpolation-induced error and is small (reasonably close to unity) for all N; that A^N is very well conditioned; and that the error estimator effectivity is quite close to unity and sharper as I increases.

4.3. Example 3: a sensor placement problem

With this example, we aim to demonstrate the application of the present method to optimal sensor placement for field reconstruction of parametrized systems. In particular, we consider the problem of placing a number of sensors in the spatial domain to obtain experimental measurements of a parametrized time-dependent physical field (e.g. temperature, flow, pressure, and energy) and of reconstructing the entire field variable from the obtained experimental data. This problem has been studied by many authors [21–26] in the context of distributed process systems in which the physical field evolves with time t.

The particular example considered is a channel flow past a unit circular cylinder for a Reynolds number variation in the range $\mathscr{D}^{Re} \equiv [100, 200]$. This example has also been investigated in [21, 26] for a particular Reynolds number of 100. Here, we consider the flow field to vary with the Reynolds number Re and evolve with time t. Direct numerical simulation (DNS) of the Navier–Stokes equations using a discontinuous Galerkin method [27] is performed to compute the flow field.

An unstructured two-dimensional grid with 30 070 nodes and 3007 cubic elements is used in the computation. The grid is extended from 10 cylinder diameters to 15 cylinder diameters in the horizontal direction, and ± 10 cylinder diameters in flow normal direction. The timestep Δt between two consecutive snapshots is five times the simulation timestep of 0.05 s, i.e. $\Delta t = 0.25$. We shall consider the horizontal velocity component $U(x; Re, t^j)$ and use the 'synthetic' data provided by the DNS solver.

The goal is to determine the optimal locations of sensors, thereby allowing accurate reconstruction of the velocity $U(x; Re, t^j)$ for any given Re in the range $\mathscr{D}^{Re}$ and time-discrete level $t^j = j\Delta t, 1 \leqslant j \leqslant J = 40$. To achieve this goal, we first employ the DNS solver to obtain $\mathscr{V}_K = \{U_k, 1 \leqslant k \leqslant K\}$ which consists of $K = 240$ solutions obtained for Reynolds numbers of 100, 120, 140, 160, 180, and 200. Note that $J = 40$ solutions are obtained in time for each Reynolds number. We next create a set of mean-deviated solutions as $\mathscr{U}_K = \{\zeta_k = U_k - \overline{U}, 1 \leqslant k \leqslant K\}$, where $\overline{U} = (1/K)\sum_{k=1}^{K} U_k$ is the mean solution. Based upon $\mathscr{U}_K$, we construct the KL basis set $\{\phi_n\}_{n=1}^{N}$, the interpolation point set $\{z_n\}_{n=1}^{N}$, and the cardinal basis set $\{\psi_n\}_{n=1}^{N}$. Now for a given new velocity U, we compute its best approximation as

$$U_N^* = \overline{U} + \sum_{n=1}^{N} (\phi_n, U - \overline{U})\phi_n$$

and its coefficient-function approximation as

$$U_N = \overline{U} + \sum_{n=1}^{N} (U(z_n) - \overline{U}(z_n))\psi_n$$

We see that U_N^* requires the velocity U everywhere in the spatial domain, whereas U_N can be constructed from known ('experimental') values only at the interpolation points, $U(z_n), 1 \leqslant n \leqslant N$. Hence, reconstruction of the velocity field from experimental measurements with the best approximation approach is not practical. Below we present numerical results obtained with our interpolation approach.

Figure 3 shows the first two KL basis functions. We further show in Figure 4 the distribution of the hierarchical points and best points on the domain for $N = 30$. In both cases, the points are
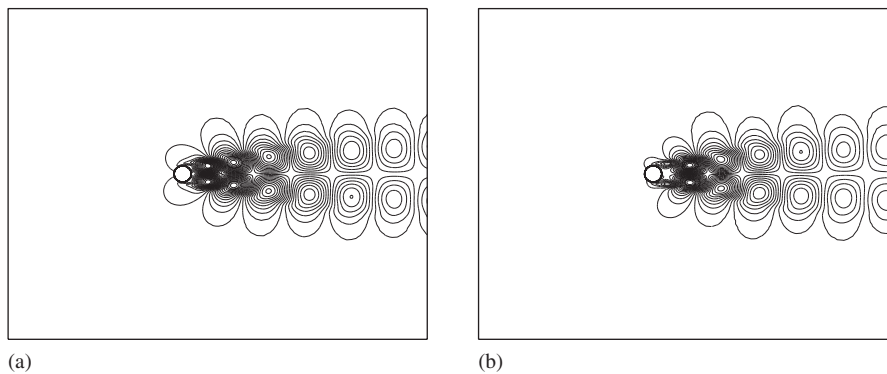

(a)   (b)

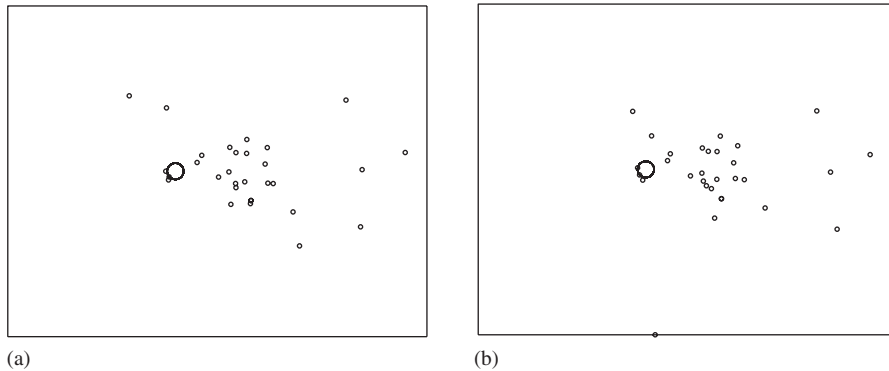Figure 3. Contour plot of the first two KL basis functions: (a) ϕ_1 and (b) ϕ_2.

Figure 4. Distribution of the sensors on the physical domain for $N = 30$: (a) the hierarchical points and (b) the best points.

Table VIII. Numerical results for the reconstruction of $U(\cdot; Re, t^j)$ using the HPIM: $\varepsilon^*_{N,\max,\mathrm{rel}}$, $\varepsilon_{N,\max,\mathrm{rel}}$, $\overline{\Upsilon}_N$, $\overline{\eta}_{N,1}$, $\overline{\eta}_{N,3}$, and $\overline{\eta}_{N,5}$ as a function of N.

N	$\varepsilon^*_{N,\max,\mathrm{rel}}$	$\varepsilon_{N,\max,\mathrm{rel}}$	$\overline{\Upsilon}_N$	$\overline{\eta}_{N,1}$	$\overline{\eta}_{N,3}$	$\overline{\eta}_{N,5}$
5	4.16E−02	5.47E−02	1.13	0.54	0.86	0.94
10	1.36E−02	1.67E−02	1.34	0.47	0.75	0.84
15	5.92E−03	7.04E−03	1.33	0.32	0.77	0.87
20	2.76E−03	4.05E−03	1.45	0.30	0.64	0.78
25	1.69E−03	3.58E−03	1.74	0.36	0.59	0.77
30	1.22E−03	2.90E−03	1.92	0.33	0.66	0.83

mostly distributed in the wake region right behind the cylinder. This is because in that region the velocity U varies most significantly as observed in Figure 3. It is also interesting to note that there is one best point on the lower boundary.

We now introduce a parameter test sample Ξ_{Test} of size $Q_{\mathrm{Test}} = 400$ including 10 Reynolds numbers {100, 110, 120, 130, 140, 160, 170, 180, 190, 200} in combination with 40 time-discrete levels. We next tabulate, as a function of N, $\varepsilon^*_{N,\max,\mathrm{rel}}$, $\varepsilon_{N,\max,\mathrm{rel}}$, $\overline{\Upsilon}_N$, and $\overline{\eta}_{N,I}$, $I = 1, 3, 5$, in Table VIII for the HPIM and in Table IX for the BPIM; here $\varepsilon^*_{N,\max,\mathrm{rel}} = \max_{(Re,t^j) \in \Xi_{\mathrm{Test}}}$ $\varepsilon^*_N(Re, t^j)/\|U(\cdot; Re, t^j)\|$, $\varepsilon_{N,\max,\mathrm{rel}} = \max_{(Re,t^j) \in \Xi_{\mathrm{Test}}} \varepsilon_N(Re, t^j)/\|U(\cdot; Re, t^j)\|$, $\overline{\Upsilon}_N = Q_{\mathrm{Test}}^{-1}$ $\sum_{(Re,t^j) \in \Xi_{\mathrm{Test}}} \varepsilon_N(Re, t^j)/\varepsilon^*_N(Re, t^j)$, and $\overline{\eta}_{N,I} = Q_{\mathrm{Test}}^{-1} \sum_{(Re,t^j) \in \Xi_{\mathrm{Test}}} \eta_{N,I}(Re, t^j)$. In both cases, the average error ratio $\overline{\Upsilon}_N$ is less than 2 and the error estimator effectivity is closer to unity and sharper as I increases. The *a posteriori* error estimator is crucial for this problem: first, it allows us to use a 'minimal' number of sensors while satisfying the desired accuracy; second, it eliminates some uncertainty in the obtained results.

For this problem, the HPIM results are just slightly less accurate than the BPIM results for a fixed dimension N. However, in application, the HPIM can be much more economical than the BPIM. More specifically, we let $N_{\max}$ be the basis dimension for which the condition $\hat{\varepsilon}_{N_{\max},I}(Re, t^j) \leqslant \varepsilon_{\mathrm{tol}}$ is satisfied for all possible parameter values; here $\varepsilon_{\mathrm{tol}}$ is the desired tolerance. For a given parameter

Table IX. Numerical results for the reconstruction of $U(\cdot; Re, t^j)$ using the BPIM: $\varepsilon^*_{N,\max,rel}$, $\varepsilon_{N,\max,rel}$, $\overline{\Upsilon}_N$, $\overline{\eta}_{N,1}, \overline{\eta}_{N,3}$, and $\overline{\eta}_{N,5}$ as a function of N.

N	$\varepsilon^*_{N,\max,rel}$	$\varepsilon_{N,\max,rel}$	$\overline{\Upsilon}_N$	$\overline{\eta}_{N,1}$	$\overline{\eta}_{N,3}$	$\overline{\eta}_{N,5}$
5	4.16E−02	4.65E−02	1.09	0.51	0.85	0.94
10	1.36E−02	1.54E−02	1.23	0.39	0.66	0.78
15	5.92E−03	8.26E−03	1.22	0.37	0.75	0.87
20	2.76E−03	3.81E−03	1.33	0.36	0.67	0.81
25	1.69E−03	3.33E−03	1.54	0.38	0.57	0.72
30	1.22E−03	2.03E−03	1.85	0.30	0.56	0.69

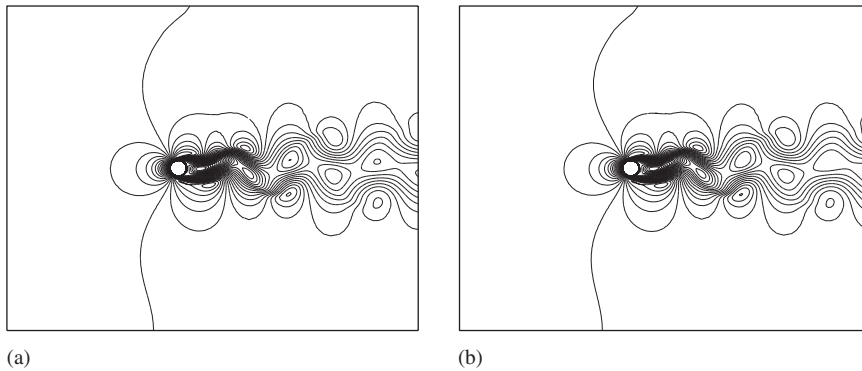(a)   (b)

Figure 5. Reconstruction of the velocity $U(x; Re, t^j)$ using the BPIM: (a) the exact velocity for $Re = 130$ and $t^j = 40\Delta t$ and (b) the reconstructed velocity $U_N(\cdot; Re, t^j)$ for $N = 20$.

value (Re, t^j), we would like to choose N in the range $[1, N_{\max}]$ as the smallest dimension satisfying $\hat{\varepsilon}_{N,I}(Re, t^j) \leqslant \varepsilon_{tol}$. We thus need to construct $Z^{bpt}_{N,I}$ for all N ($\leqslant N_{\max}$) or, in general, a total number of $(N_{\max} + I)(N_{\max} + I + 1)/2$ BPIM sensors, since the best points are not hierarchical. However, we would need only $N_{\max} + I$ sensors with the HPIM. The HPIM can thus save substantial cost and time for the experimental setup, as the total number of sensors required is $(N_{\max} + I + 1)/2$ times smaller than that of the BPIM.

Finally, we look at the reconstruction of $U(\cdot; Re, t^j)$ for $Re = 130$ and $t^j = 40\Delta t$ shown in Figure 5(a); note that this solution is not included in $\mathscr{U}_K$. We present in Figure 5(b) its reconstructed field obtained with the BPIM for $N = 20$. In addition, we show the reconstruction in Figure 6(a) for $N = 10$ and in Figure 6(b) for $N = 20$ obtained using the HPIM. We see that only 10 HPIM sensors are enough to capture almost all the important features of the actual field, and that, with 20 HPIM sensors, the reconstructed field is almost indistinguishable from the actual field. Similar results are in fact observed for all (Re, t^j) in Ξ_{Test}.

In summary, we obtain encouraging results with few sensors placed on the domain. However, we have not addressed sensitivity of the reconstruction with respect to noise in data and have not incorporated uncertainty information into the reconstruction process. These extensions will
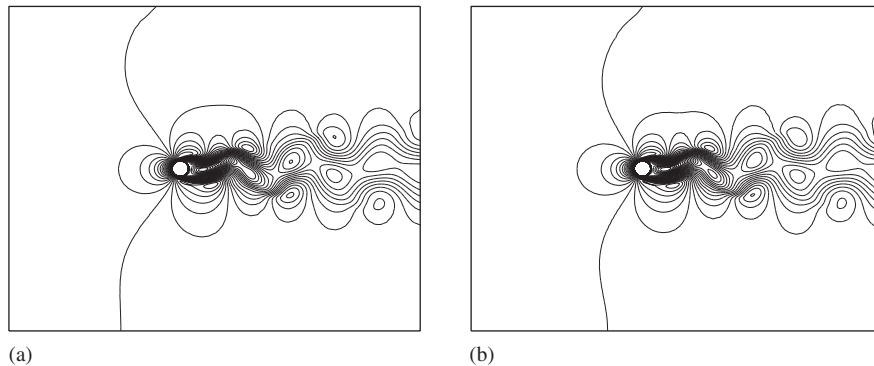
(a)   (b)

Figure 6. Reconstruction of $U(\cdot; Re, t^j)$ for $Re = 130$ and $t^j = 40\Delta t$ using the
HPIM: (a) $N = 10$ and (b) $N = 20$.

be discussed in detail in a future paper devoted to not only field reconstruction but also the measurement of engineering outputs.

5. CONCLUSIONS

We have presented an interpolation method for the efficient and accurate approximation of parametrized functions *via* an appropriate basis set and an associated (almost) optimal interpolation point set. In particular, rather than general basis sets such as polynomials, we construct a specific problem-dependent basis set with superior approximation properties of parametrized functions. At the heart of our method is the formulation of a least-squares error minimization which can be solved efficiently by standard optimization algorithms to yield the best interpolation points. We have compared our method with the EIM and investigated its performance relative to the best approximation. The BPIM outperforms the EIM and yields approximations which are very close to the best approximations. In addition, we have quantified the approximation error with *a posteriori* error estimators. Our error estimates are inexpensive and quite sharp. The numerical results presented in the paper demonstrate our claims.

APPENDIX A

A.1. The empirical interpolation method

We describe the empirical interpolation procedure developed in [15, 16] for the approximation of the parameter-dependent function $u(x; \mu)$. The EIM consists of a 'greedy' selection process for generating a basis set with good approximation properties and a simple algorithm for selecting the interpolation points.

The greedy selection process is used to select maximally independent basis set $\{\xi_n\}_{n=1}^N$ from the given family $\{u(\cdot; \mu_k)\}_{k=1}^K$. We first choose our first basis function to be $\xi_1 = u_{j_1}$ with $j_1 = \arg\max_{k \in \{1,\ldots,K\}} \|u(\cdot; \mu_k)\|_{L^\infty(\Omega)}$, and define $W_1^u = \mathrm{span}\{\xi_1\}$. For $L = 2, \ldots, N$, we

determine $j_L = \arg \max_{k \in \{1, \ldots, K\}} \varepsilon_{L-1}^*(\mu_k)$, and define $\xi_L(x) = u(x; \mu_{j_L})$ and $W_L^u = \mathrm{span}\{\xi_n, 1 \leqslant n \leqslant L\}$; here for $k = 1, \ldots, K$, $u_{L-1}^*(\cdot; \mu_k) \equiv \arg \min_{w \in W_{L-1}^u} \|u(\cdot; \mu_k) - w\|_{L^\infty(\Omega)}$ and $\varepsilon_{L-1}^*(\mu_k) \equiv \|u(\cdot; \mu_k) - u_{N-1}^*(\cdot; \mu_k)\|_{L^\infty(\Omega)}$. In essence, W_L^u comprises basis functions from the family $\mathcal{U}_K$. For $u(x; \mu)$ of finite dimension, the optimization for $u_{L-1}^*(x; \mu_k)$ and hence $\varepsilon_{L-1}^*(\mu_k)$ is a *standard linear program*. In actual practice, rather than the $L^\infty(\Omega)$-norm, the $L^2(\Omega)$-norm surrogate is used in the best approximation, and the construction of $\{\xi_n\}_{n=1}^N$ is considerably less expensive.

Next a set of interpolation points, $Z_N^{\mathrm{mp}} = \{z_1^{\mathrm{mp}}, \ldots, z_N^{\mathrm{mp}}\}$, is constructed as follows. We first set $z_1^{\mathrm{mp}} = \arg \mathrm{ess} \sup_{x \in \Omega} |\xi_1(x)|$, $q_1(x) = \xi_1(x)/\xi_1(z_1^{\mathrm{mp}})$, $B_{11}^1 = 1$. Then for $L = 2, \ldots, N$, we solve the linear system $\sum_{j=1}^{L-1} \sigma_j^{L-1} q_j(z_i^{\mathrm{mp}}) = \xi_L(z_i^{\mathrm{mp}})$, $1 \leqslant i \leqslant L - 1$, and set $r_L(x) = \xi_L(x) - \sum_{j=1}^{L-1} \sigma_j^{L-1} q_j(x)$, $z_L^{\mathrm{mp}} = \arg \mathrm{ess} \sup_{x \in \Omega} |r_L(x)|$, $q_L(x) = r_L(x)/r_L(z_L^{\mathrm{mp}})$, and $B_{ij}^L = q_j(z_i^{\mathrm{mp}})$, $1 \leqslant i, j \leqslant L$. Clearly, the EIM point set Z_N^{mp} is hierarchical, and inexpensive to construct.

Then, for any given $\mu \in \mathcal{D}$, $u(x; \mu)$ may be approximated by a coefficient-function expansion $u_N(x; \mu) = \sum_{n=1}^N \varphi_{Nn}(\mu) q_n(x)$, where $\sum_{j=1}^N B_{ij}^N \varphi_{Nj}(\mu) = u(z_i^{\mathrm{mp}}; \mu)$, $1 \leqslant i \leqslant N$, and $B_{ij}^N = q_j(z_i^{\mathrm{mp}})$.

A.2. Karhunen–Loève procedure

We describe the KL expansion to generate $\{\phi_n\}_{n=1}^N$ from the given family $\{\zeta_k\}_{k=1}^K$. First, a two-point spatial correlation function is defined as

$$\mathcal{K}(x, x') = \frac{1}{K} \sum_{k=1}^K \zeta_k(x) \zeta_k(x') \tag{A1}$$

which accepts the following spectral decomposition:

$$\mathcal{K}(x, x') = \sum_{k=1}^K \lambda_k \phi_k(x) \phi_k(x') \tag{A2}$$

Here the set of basis functions ϕ_k, $1 \leqslant k \leqslant K$, are ordered such that the associated eigenvalues

$$\lambda_k = \frac{1}{K} \sum_{l=1}^K (\phi_k, \zeta_l)^2 \tag{A3}$$

satisfy $\lambda_k \geqslant \lambda_{k+1}$.

Next, for a given $N \leqslant K$, the KL procedure consists in finding ϕ_n, $1 \leqslant n \leqslant N$, so as to maximize the captured energy

$$\max E_N = \sum_{n=1}^N \left(\frac{1}{K} \sum_{k=1}^K (\phi_n, \zeta_k)^2 \right) = \sum_{n=1}^N \lambda_n \tag{A4}$$

subject to the constraints $(\phi_n, \phi_{n'}) = \delta_{nn'}$, $1 \leqslant n, n' \leqslant N$. The first few basis functions thus represent the main energy-containing structures in the snapshots, with their relative importance quantified by λ_n. It can be shown that the problem (A4) amounts to solving the eigenfunction equation the problem (A4) amounts to solving the eigenfunction equation

$$(\mathcal{K}(x, x'), \phi(x')) = \lambda \phi(x) \tag{A5}$$

for the first N eigenfunctions.

The method of snapshots [19] expresses a typical empirical eigenfunction $\phi(x)$ as a linear combination of the ζ_k:

$$\phi(x) = \sum_{k=1}^{K} a_k \zeta_k(x) \tag{A6}$$

Inserting this representation and (A1) into (A5), we immediately obtain

$$Ca = \lambda a \tag{A7}$$

where $C \in \mathbb{R}^{K \times K}$ is given by $C_{ij} = (1/K)(\zeta_i, \zeta_j), 1 \leqslant i, j \leqslant K$. Eigenproblem (A7) can then be solved for the first N eigenvectors from which the KL basis functions ϕ_n, $1 \leqslant n \leqslant N$, are constructed by (A6).

The optimality of the KL basis can be shown by considering an approximate representation $\hat{\zeta}_k(x) = \sum_{n=1}^{N} \gamma_{Nn}^k \varphi_n(x)$ of $\zeta_k(x)$ for an arbitrary set of orthonormal basis functions, $\{\varphi_n\}_{n=1}^{N}$, and demonstrating that the KL basis is a minimizer of the error minimization problem

$$\min \sum_{k=1}^{K} \left\| \zeta_k - \sum_{n=1}^{N} \gamma_{Nn}^k \varphi_n \right\|^2 \tag{A8}$$

Indeed, this minimization problem is equivalent to the maximization problem (A4), which in turn asserts the optimality of $\{\phi_n\}_{n=1}^{N}$. Furthermore, the average least-squares error can be calculated as

$$\frac{1}{K} \sum_{k=1}^{K} \left\| \zeta_k - \sum_{n=1}^{N} (\phi_n, \zeta_k)\phi_n \right\|^2 = \sum_{j=N+1}^{K} \lambda_j \tag{A9}$$

Expression (A9) gives us an idea for choosing N as the smallest integer such that $\sum_{n=1}^{N} \lambda_n / \sum_{k=1}^{K} \lambda_k \geqslant 0.99$.

REFERENCES

1. Nguyen NC, Peraire J. An interpolation method for the reconstruction and recognition of face images. *Proceedings of the 2nd International Conference on Computer Vision Theory and Applications*, Barcelona, Spain, 2007.
2. Nguyen NC, Peraire J. An efficient reduced-order modeling approach for nonlinear parameterized partial differential equations, in preparation.
3. Quarteroni A, Sacco R, Saleri F. Numerical mathematics. *Texts in Applied Mathematics*, vol. 37. Springer: New York, 1991.
4. Rivlin TJ. *An Introduction to the Approximation of Functions*. Dover: New York, 1981.
5. Erdös P. Problems and results on the theory of interpolation, ii. *Acta Mathematica Academiae Scientiarum Hungaricae* 1961; **12**:235–244.
6. Chen Q, Babuška I. Approximate optimal points for polynomial interpolation of real functions in an interval and in a triangle. *Computer Methods in Applied Mechanics and Engineering* 1995; **128**(4):405–417.

7. Brutman L. Lebesgue functions for polynomial interpolation—a survey. *Annals of Numerical Mathematics* 1997; **4**:111–127.
8. Boyd JP. A numerical comparison of seven grids for polynomial interpolation on the interval. *Computers and Mathematics with Applications* 1999; **38**:35–50.
9. Chen Q, Babuška I. The optimal symmetrical points for polynomial interpolation of real functions in the tetrahedron. *Computer Methods in Applied Mechanics and Engineering* 1996; **137**(1):89–94.
10. Taylor MA, Wingate BA, Vincent RE. An algorithm for computing fekete points in the triangle. *SIAM Journal on Numerical Analysis* 2000; **38**(5):1707–1720.
11. Heinrichs W. Improved Lebesgue constants on the triangle. *Journal of Computational Physics* 2005; **207**(2): 625–638.
12. Luo H, Pozrikidis C. A Lobatto interpolation grid in the tetrahedron. *IMA Journal of Applied Mathematics* 2006; **71**(2):298–313.
13. Womersley RS, Sloan IH. How good can polynomial interpolation on the sphere be. *Advances in Computational Mathematics* 2001; **14**(3):195–226.
14. Hesthaven JS. From electrostatics to almost optimal nodal sets for polynomial interpolation in a simplex. *SIAM Journal on Numerical Analysis* 1998; **35**(2):655–676.
15. Barrault M, Maday Y, Nguyen NC, Patera AT. An 'empirical interpolation' method: application to efficient reduced-basis discretization of partial differential equations. *Comptes Rendus de l Acadamie des Sciences Paris*, *Série I* 2004; **339**:667–672.
16. Grepl MA, Maday Y, Nguyen NC, Patera AT. Efficient reduced-basis treatment of nonaffine and nonlinear partial differential equations. *Mathematical Modelling and Numerical Analysis* (*M2AN*) 2007, to appear.
17. Maday Y, Nguyen NC, Patera AT, Pau GSH. A general, multipurpose interpolation procedure: the magic points. *Proceedings of the 2nd International Conference on Scientific Computing and Partial Differential Equations*, Hong Kong Baptist University, Hong Kong, 2005.
18. Cancès E, LeBris C, Maday Y, Nguyen NC, Patera AT, Pau GSH. Feasibility and competitiveness of a reduced basis approach for rapid electronic structure calculations in quantum chemistry. *Proceedings of the Montreal Workshop for High-dimensional Partial Differential Equations in Science and Engineering*, 2005, accepted.
19. Sirovich L. Turbulence and the dynamics of coherent structures, part 1: coherent structures. *Quarterly of Applied Mathematics* 1987; **45**(3):561–571.
20. Marquardt DW. An algorithm for least-squares estimation of nonlinear parameters. *SIAM Journal on Applied Mathematics* 1963; **11**(1):431–444.
21. Cohen K, Siegel S, McLaughlin T. Sensor placement based on proper orthogonal decomposition modeling of a cylinder wake (AIAA Paper 2003-4259). *Proceedings of the 33rd AIAA Fluid Dynamics Conference and Exhibit*, Florida, U.S.A., June 2003.
22. Alonso AA, Frouzakis CE, Kevrekidis IG. Optimal sensor placement for state reconstruction of distributed process systems. *AIChE Journal* 2004; **50**:1438–1452.
23. Mokhasi P, Rempfer D. Optimized sensor placement for urban flow measurement. *Physics of Fluids* 2004; **16**(5):1758–1764.
24. Singh AK, Hahn J. Determining optimal sensor locations for state and parameter estimation for stable nonlinear systems. *Industrial and Engineering Chemistry Research* 2005; **44**(15):5645–5659.
25. Luchtenburg M, Tadmor G, Lehmann O, Noack BR, King R, Morzynski M. Tuned pod Galerkin models for transient feedback regulation of the cylinder wake (AIAA Paper 2006-1407). *Proceedings of the 44th AIAA Aerospace Sciences Meeting and Exhibit*, Reno, Nevada, June 2006.
26. Willcox K. Unsteady flow sensing and estimation via the gappy proper orthogonal decomposition. *Computers and Fluids* 2006; **35**:208–226.
27. Persson P, Peraire J. An efficient low memory implicit dg algorithm for time dependent problems. *Proceedings of the 44th AIAA Aerospace Sciences Meeting*, Reno, Neveda, June 2006; AIAA-2006-0113.